Velocity field of the western entrance to the Barents Sea

Randi B. Ingvaldsen, Lars Asplin, and Harald Loeng
Institute of Marine Research, Bergen, Norway

Received 5 February 2003; revised 22 September 2003; accepted 15 December 2003; published 13 March 2004.

[1] By the use of 4-year long records from moored current meters between 71°30′N and 73°30′N of the western entrance to the Barents Sea, the velocity field of the Atlantic inflow is examined. The mean velocity field shows the Atlantic inflow as a wide core that occupies most of this section, but the general picture is a velocity field that is dominated by large and frequent fluctuations. The key parameter that to a large degree determines the spatial distribution of the velocity field is sea level changes within the section that are induced by the local wind field. The main process is the Ekman transport through its ability to accumulate water thereby creating strong gradients of barotropic pressure and associated currents. Southwesterly winds along the Norwegian coast and southeasterly winds farther north will, in general, create wide inflows, while northerly winds will result in wide outflows. These flow regimes may be persistent for up to 2–3 weeks and are related to the relative strength and lateral extension of the Icelandic low and the Arctic high, although the alignment of the local isobars must be considered in order to be able to describe the details of the flow. *INDEX TERMS:* 4512 Oceanography: Physical: Currents; 4219 Oceanography: General: Continental shelf processes; 4556 Oceanography: Physical: Sea level variations; *KEYWORDS:* Barents Sea, velocity field, Ekman transport, current oscillations

Citation: Ingvaldsen, R. B., L. Asplin, and H. Loeng (2004), Velocity field of the western entrance to the Barents Sea, *J. Geophys. Res.*, *109*, C03021, doi:10.1029/2003JC001811.

1. Introduction

[2] The main inflow of Atlantic Water (AW) to the Barents Sea takes place in the Norwegian Atlantic Current (NAC) through the Barents Sea Opening (BSO) (Figure 1). The hydrography along the section between Norway and Bear Island indicates a rather stable inflow of AW in the southern part and an outflow in the north (e.g., Figures 2a and 2b). Such a circulation scheme was confirmed by 2 months of current measurement that was presented by *Blindheim* [1989]. Recent publications of vessel mounted Acoustic Doppler Current Profiler (ADCP) [*Haugan*, 1999] found the inflow to be predominately barotropic and to take place in two cores with a return flow between them. The results were supported by the analyses of hydrographic measurements [*Furevik*, 2001] (see also Figures 2c and 2d) and by the additional analysis of ADCP data [*O'Dwyer et al.*, 2001]. *Ingvaldsen et al.* [2002] analyzed a 1-year time series from moored current meters and found that there were large fluctuations in both time and space of the BSO current pattern. They concluded that the flow might occur as (1) a wide Atlantic inflow, (2) a wide outflow, or (3) simultaneous inflow and outflow in distinct cores. AW may possibly also enter as a retrograde slope jet as described by *Li and McClimans* [1998] and as documented by current measurements during winter and presented by *Loeng and Sætre* [2001] or by model studies [*Ådlandsvik and Hansen*, 1998].

[3] The variability of the Atlantic inflow is considerable [*Haugan*, 1999; *Ingvaldsen et al.*, 2002], and variability in the barotropic currents that are generated by sea level gradients is important on a short timescales [*McClimans et al.*, 1999]. The variability on timescales from day to year is linked to the atmospheric fields [*Ådlandsvik and Loeng*, 1991; *Loeng et al.*, 1997], and numerical modeling has shown that stronger southwesterly winds give higher inflow and vice versa [*Ådlandsvik and Loeng*, 1991; *Furevik*, 1998]. However, the physical process controlling the flow was not identified. Questions like, "Does the wind simply change the current velocity or does it also change the current structure?" and "How can the wind cause these changes when the currents are mostly barotropic?" are still unanswered. The motivation for this investigation is to study the spatial distribution of the velocity field and to establish an explanation model that fulfils the earlier results and provide answers to the above questions. That is, it must explain that (1) the velocity field occurs as different patterns (i.e., wide inflow or wide outflow), (2) the velocity field is predominately barotropic, and (3) the inflow increases with increasing southwesterly wind and vice versa. To do so, we use 4-year- long records from an array of moored current meters across the southern part of the BSO. Data and analysis techniques are described in section 2, while section 3 gives a brief description of a few days of fluctuations in the velocity field and examines the forcing behind them. A statistical approach to explaining the spatial distribution within the velocity field is provided in section 4, and the relationship between the flow field and the atmo-

0148-0227/04/2003JC001811$09.00

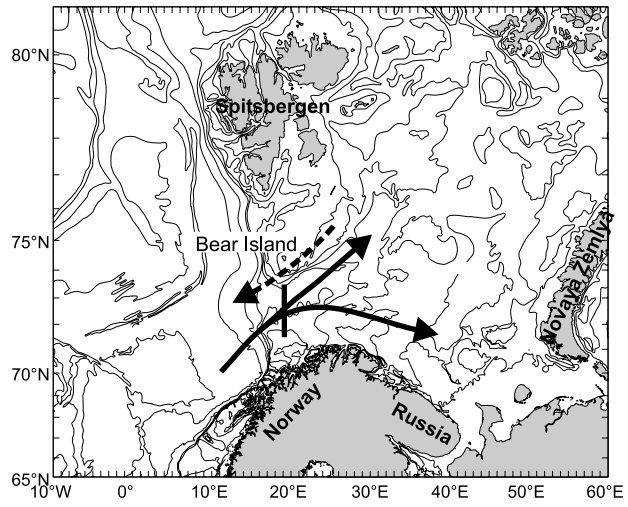

Figure 1. Map of the Barents Sea. The solid and dashed arrows indicate flow of Atlantic water (AW) and Arctic water, respectively. The solid line indicates the section where the current meter moorings were deployed.

spheric and sea level fields are investigated. A brief summary and conclusions are given in section 5.

2. Data and Analysis

[4] The data material consists of velocity and temperature measurements from moored Aanderaa current meters RCM7 from August 1997 to August 2001. The moorings were deployed between 71°30′N and 73°30′N, and mainly covered the Atlantic inflow but not the coastal inflow and the flows on the slope south of Bear Island (Figure 2). The number of moorings deployed, the distance between the moorings, and the number of instruments on each mooring, varied throughout the period (Table 1 and Figure 3). Data were recorded every 20 min. To fill gaps in the time series due to missing single instruments (Figure 3), simple linear interpolation of the velocities from the instrument above and/or below was performed. This is an adequate method since the velocities are mostly barotropic [e.g., *Haugan*, 1999]. When moorings 2b and 3b were not deployed, interpolated values from the two surrounding moorings were used. In addition, time filtering was performed with an order 4 Butterworth lowpass filter [*Roberts and Roberts*, 1978].

[5] The general problem with an array of moorings is the limited spatial resolution, and mesoscale eddies may be a problem because they often are only partly captured by the moorings. Such partly captured eddies will turn up as fluctuations with timescales of several days, which are not correlated between adjacent moorings, and will give large differences between transport series calculated with different spatial resolution. Our transport series sensitivity to increased resolution has been tested [*Ingvaldsen et al.*, 2004], and the results indicated that by using a 14 days filter, most of the effects of the unresolved mesoscale perturbations were eliminated. This means that a time filter is necessary to remove the spatial structures the array of moorings do not resolve. The data material was therefore filtered by removing fluctuations with periods that were less than 14 days before empirical orthogonal functions (EOF) analysis was performed. Owing to the length of the time series, any sporadic mesoscale eddies still remaining in the time series (because they have timescales longer than 14 days) will only contribute significantly in the EOF analysis if they appear at fixed locations. If this were the situation, they would have had to be generated within the area or transported along a certain depth contour. Such eddies might be generated in the shear zone between the inflowing and the outflowing waters of the Bear Island Trough, but it is unlikely that these can persist long enough as not to be removed by the time filtering. This is supported by *Loeng and Sætre* [2001], who found that the eddies in the area seem to be rather limited in both time and space.

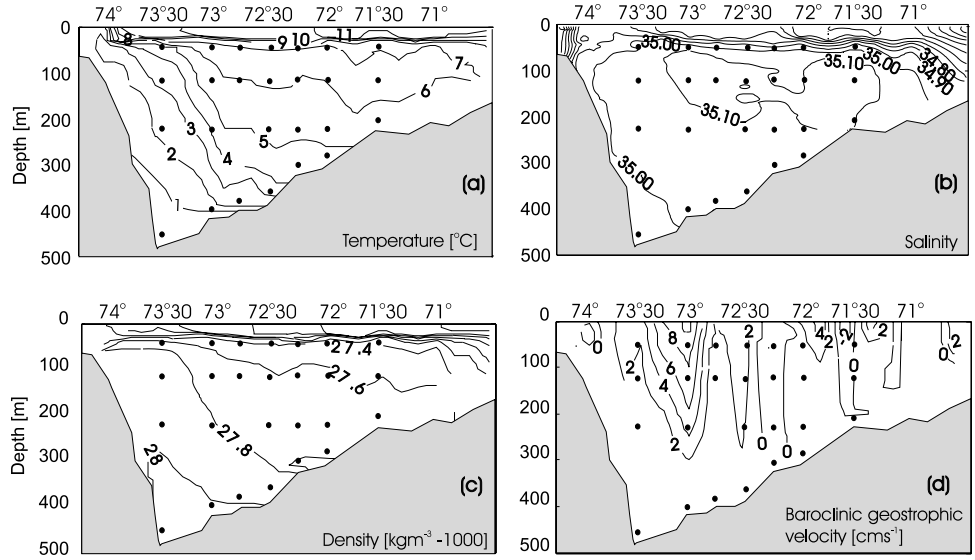

Figure 2. (a) Temperature, (b) salinity, (c) density, and (d) baroclinic geostrophic velocity in August 1998 and location of all the instruments (dots). Table 1 and Figure 3 give the information of the moorings and instruments deployed at a given time.

Table 1. Mooring Details and Statistics for the Current Meters

Mooring	Position	Days of Record	Depth, m		Mean of Velocity		Kinetic Energy		Temperature, °C
			Water	RCM	Magnitude, cm s^{-1}	Direction, deg	Mean, g cm s^{-1} s^{-1}	Fluctuations, g cm s^{-1} s^{-2}	
1	71°30′N 19°47′E	467	227	50	4.3	123	7	152	6.5
		659		125	3.8	129	6	144	6.2
		834		212	3.9	134	6	90	5.8
2	72°00′N 19°39′E	865	309	50	4.3	123	8	109	6.5
		872		125	4.4	131	9	101	5.9
		624		225	4.0	134	8	106	5.7
		1077		294	3.5	139	7	78	4.9
2b	72°15′N 19°35′E	199	324	50	2.2	66	2	86	6.5
		368		125	2.0	24	2	86	5.8
		199		225	2.8	55	2	80	5.7
		567		310	2.7	50	4	50	4.5
3	72°30′N 19°32′E	905	388	50	3.4	120	6	137	6.1
		908		125	3.5	117	7	131	5.7
		1060		225	3.6	114	6	115	5.2
		1280		375	3.2	101	5	77	3.1
3b	72°45′N 19°32′E	275	392	50	2.5	141	13	116	5.3
		171		125	4.4	155	8	69	5.1
		171		385	3.4	171	4	56	2.9
4	73°00′N 19°33′E	657	419	50	2.2	124	1	170	5.8
		1194		125	2.6	113	2	155	5.3
		543		225	2.1	118	1	135	4.2
		705		401	0.8	130	0	119	2.3
5	73°30′N 19°20′E	414	480	50	1.7	190	1	169	4.9
		1082		125	1.9	209	1	151	4.2
		715		225	5.0	224	8	120	3.2
		1082		464	7.8	227	29	78	1.5

[6] Owing to the lack in the number of moorings (Figure 3), the periods January–February 1999 and September 1999 to August 2000 were not included in the EOF analysis. For the period March–August 1999 mooring 1 was missing, and values from mooring 2 were used to represent this mooring prior to the EOF analysis. As the EOF analysis requires data from all points in time, the separate time series were concatenated before analysis, and the resulting time series were 34 months long. After the analysis, the principal components (the time series of each EOF) were split into their actual time. Owing to the concatenation, a thorough analysis of the principal components is not suitable. Conventional EOF analysis is limited by a number of factors, including the lumping together of variability over all frequency bands, and the method therefore works best when the variability is over a broad range of frequencies. Spectral analysis, on the other hand, which often is used to identify dominating timescales in a data set, works best when the variability is in narrow frequency bands. Consequently, this method cannot be expected to give good results on the same data set as conventional EOF analysis, and it did not do so (see also section 4.4).

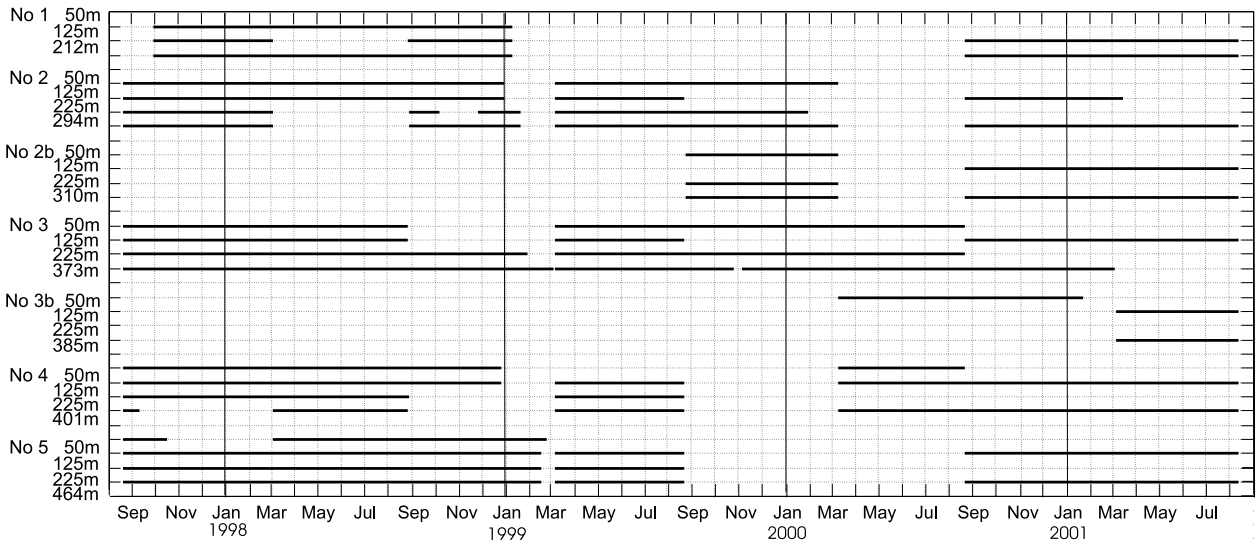

Figure 3. Time series of functioning time for each current meter.

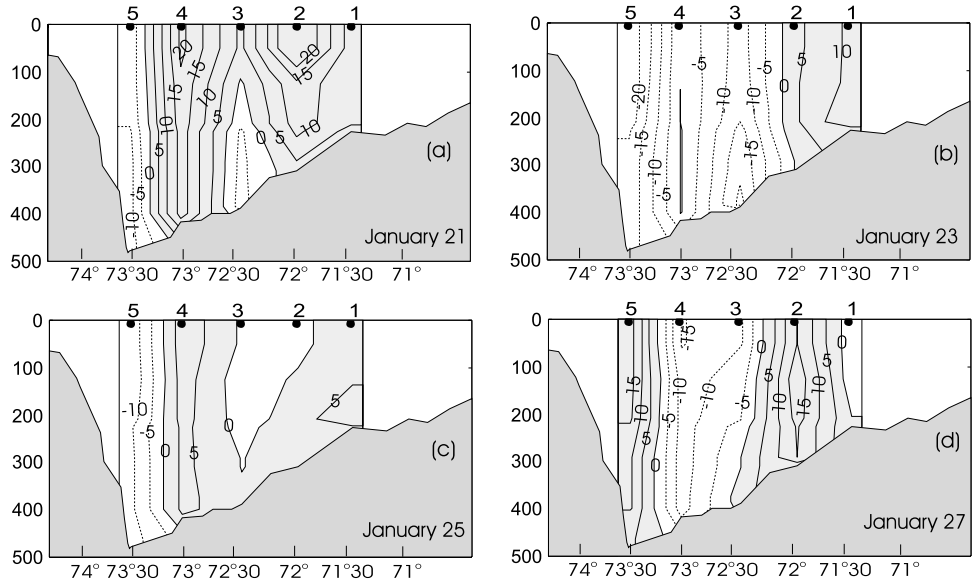

Figure 4. Vertical sections showing daily mean cross-sectional currents (cm s^{-1}) at four dates in January 1998. Shaded areas show eastward flow (i.e., flow into the Barents Sea).

[7] The atmospheric sea level pressure and wind field in 10 m above sea level were taken from the Norwegian Meteorological Institute (Met.no) hindcast archive (updated from *Eide et al.* [1985]). The sea level height was obtained from numerical simulations that were carried out with NORWECOM [*Skogen and Søiland*, 1998], which is a 3-D, primitive equation, sigma-coordinate coastal ocean model based on the Princeton Ocean Model [*Blumberg and Mellor*, 1987]. The model domain covered the Nordic Seas, the Barents Sea, and the Arctic Ocean and was discretized on a 20-km horizontal polar stereographic grid. The model forcing included initial and boundary conditions from The Norwegian Meteorological Institute-Institute of Marine Research diagnostic climatology [*Engedahl et al.*, 1998], realistic meteorological forcing from the NCEP-NCAR reanalysis project, and monthly mean river runoff and tidal forcing. The model has been validated for the BSO [*Asplin et al.*, 1998], and the results showed that the produced velocity fields in general are qualitatively good, but the magnitudes of currents are underestimated. As the sea level height in the model is calculated from the estimated currents, we expect the sea level height pattern to be realistic but with possibly underestimated gradients.

3. Short-Time Fluctuations in the Velocity Field

3.1. A Basic Description

[8] To illustrate the large variability in the velocity fields of the BSO, the period 21–27 January 1998 is investigated (Figure 4). Large fluctuations in the cross-sectional flow occurred, and from one day to another, the current was reversed in large parts of the section. On January 21, the inflow took place in two relatively strong cores with a small outflow close to the bottom in between them. Two days later, the flow had changed direction toward the Norwegian Sea all the way south to 72°N. During the next few days, there was at first a wide core of inflow with an area of stagnant water in the middle and then an inflow and outflow simultaneously in cores. The maximum velocities were about 20 cm s^{-1} in both directions. The mean velocity field indicates that the core of Atlantic inflow is located in the area near 72°30′N (Figure 5), but the daily velocity fields reveal that the location of the inflow core is not stable at this location as there may also be an outflow there. This reflects a fluctuating nature of the location of the core, as it moves laterally in and out of the domain of the current meter. The temperature recordings from the mooring at 72°30′N reveal this feature very clearly (Figure 6). It is striking how the instrument near the bottom showed much higher temperature variability than the instruments higher in the water column. At the bottom, the temperature changed more than 3°C between successive days.

[9] The high variability of the flow can also be seen from the kinetic energy computations (Table 1). The kinetic energy of the mean flow is quite low and an order of magnitude less than the kinetic energy of the flow fluctuations, which, in general, indicates weak mean flows. Mooring 4 and the three upper instruments on mooring 5 have the highest magnitude of kinetic energy of the flow fluctuations but closer to zero kinetic energy of the mean flow. These moorings were deployed in the area of the northern boundary of the AW inflow, and the spatial variability in this boundary is substantial [*Ingvaldsen et al.*, 2002]. The instrument in the deepest parts of the Bear Island Trough differs from the remainder by having a significantly higher kinetic energy of the mean flow and a relatively low magnitude of kinetic energy of the flow fluctuations. This instrument clearly captures the deep outflows from the Barents Sea.

3.2. Wind and Sea Level as Driving Mechanisms

[10] The daily mean wind field and the modeled sea level from the 7-day period in January 1998 reveal high variability in both time and space (Figure 7). On 21 January, there were strong southwesterly winds across the section. Because the Ekman transport is to the right of the wind

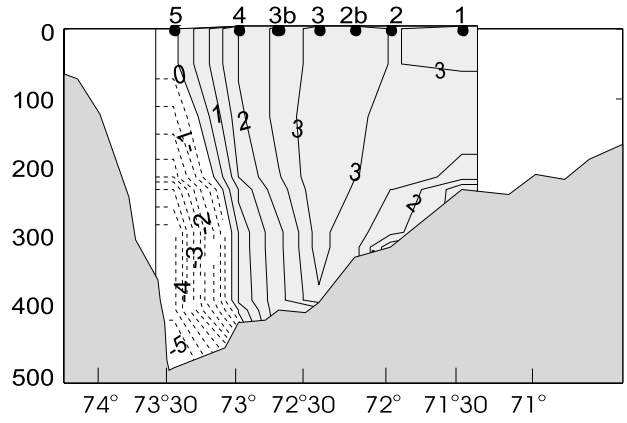

Figure 5. Mean cross-sectional velocity (cm s^{-1}). Shaded areas show eastward flow (i.e., flow into the Barents Sea).

direction, this will give an inflow in most of the section, which is consistent with the velocity field observed that day (Figure 4a). The situation on 23 January was the opposite: Strong northerly winds resulted in a westward Ekman transport, and an outflow was observed across most of the section on that day (Figures 7 and 4b). On 25 January, the winds were weak southwesterlies in the southern part and weak southeasterlies in the northern parts (Figure 7c). The associated Ekman transport would be an inflow in the south and an outflow in north and otherwise low velocities, which are highly consistent with the observed velocity field (Figure 4c). The situation on 27 January, with strong flow in narrow cores seems to be forced by winds with an easterly component (Figures 4 and 7d), although the actual physical explanation is not clear.

[11] In summary, there seems to be consistency between the direct Ekman transport and the observed currents, with an inflow that is created by southerly winds and an outflow by northerly winds. However, owing to the barotropic nature of the currents, this does not fully explain the observed velocity fields and will be investigated in section 4.

4. A Statistical Approach for the Explanation of the Velocity Fields

[12] To investigate the relation between the spatial distribution of the velocity fields and the wind, the cross-sectional velocities were decomposed by conventional EOF analysis [e.g., *Emery and Thomson*, 1997]. The advantage of EOF analysis is that it provides a compact description of the spatial and temporal variability of data series in terms of orthogonal functions or statistical "modes." Usually, most of the variance of a spatially distributed data series is in the first few modes whose pattern may then be linked to possible dynamic mechanisms. The mean of the time series were removed prior to the EOF analysis, and the time series were normalized by the standard deviation. The EOF analysis was not sensitive to the length of the time series or to the inclusion of moorings 2b and 3b (i.e., whether the analyses were performed for five or seven moorings, not shown). The leading EOF accounts for 34% of the variance in the flow field and is, according to the criterion of *North et al.* [1982], well separated from the second-order EOF explaining 20%. However, the second and third orders EOF are not well separated, and as the uniqueness failure means that the combined effect of any number of the modes must be considered, they will not be presented here. The leading EOF has a unipole pattern with a core near 72°30′N (Figure 8). Owing to both a positive and negative principal component, the EOF1 also represents situations when the current anomalies are reversed. Thus the negative state of EOF1 represents a situation with an anomalously wide outflow.

4.1. Physical Interpretation of the EOF

[13] EOF analysis is a purely statistical method, and to justify the physical interpretation of the leading EOF, we used a simple and indirect method. First, characteristics in the wind field anomalies and the sea level anomalies across the section were identified for the positive and negative state of EOF1. (As the EOF represents flow anomalies, wind and sea level anomalies are the appropriate parameters to investigate.) Then inferences on the driving mechanisms were made based on the observed characteristics. To identify the characteristics for the positive state, the times where the principal component exceed a specified value and had a positive gradient (to capture the build-up period) were found. The specified values were chosen subjectively so that only the strongest appearances of the EOF were included (the dotted horizontal line in Figure 8b), and the mean wind and sea level fields for these times were constructed. To examine whether the pressure gradient associated with the sea level could create the velocity fields pictured by the EOF, the barotropic geostrophic velocity based on the mean sea level gradient was found. The same procedure was applied to find the characteristics of the negative state of the EOF, at the times when the principal component was below a specified value and further decreasing. As for the velocity time series, the time series of the atmospheric fields and sea level fields were filtered to remove fluctuations of periods that were less than 14 days prior to the calculation of the mean.

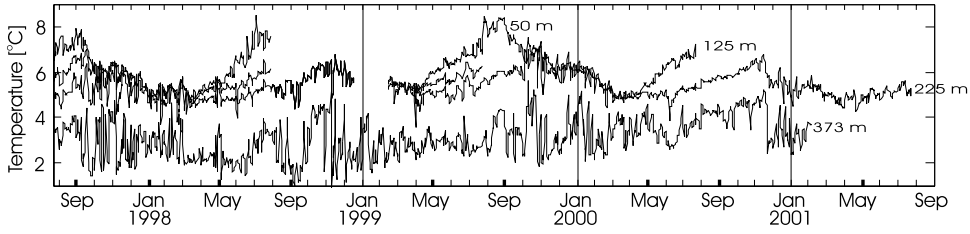

Figure 6. Daily mean temperature recordings from the mooring at 72°30′N.

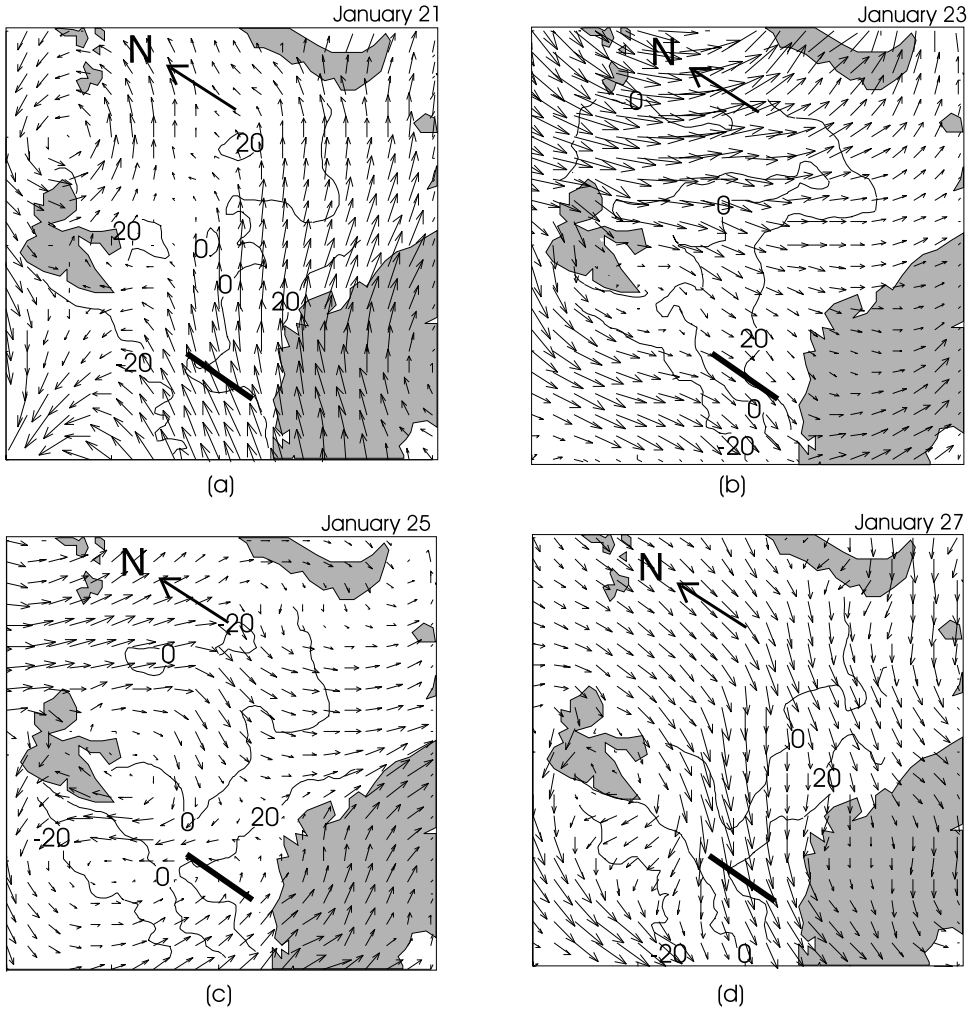

Figure 7. Daily mean wind and sea level (cm) for the same days as shown in Figure 4. Location of mooring array is indicated.

[14] The mean (anomalous) wind field during the buildup of the positive state of EOF1 (Figure 9a) is southwesterlies in the southern part of the section and southerlies in the northern part. This will create a direct Ekman transport eastward on most of the section. More importantly, the southwesterly winds in the southern part of the section will give an Ekman transport toward the Norwegian coast, while the southerly winds in the northern part will give an easterly Ekman transport. This causes a higher water level in the south than in the north, reflected in the mean sea level anomaly at times for dominating positive EOF1 (Figure 9b). The geostrophic currents associated with this sea level

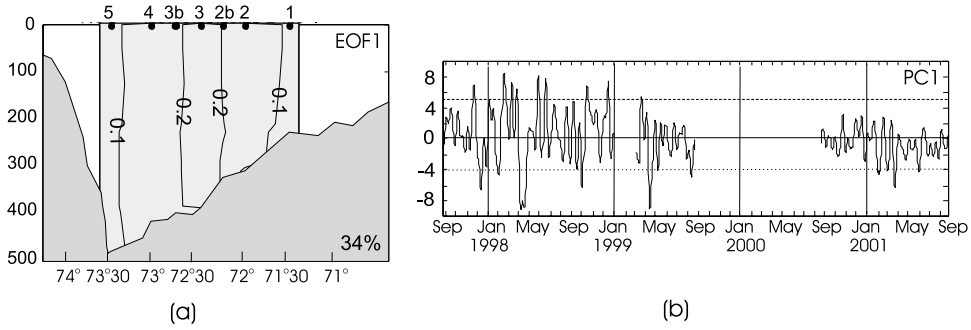

Figure 8. (a) Leading EOF for cross-sectional velocity and (b) the associated principal component. Shaded areas show eastward flow. The dotted horizontal lines in the principal component show the specified values from which the characteristics for the EOF have been taken. Note that the mean velocity was subtracted prior to the analysis, and the time series were normalized by the standard deviation.

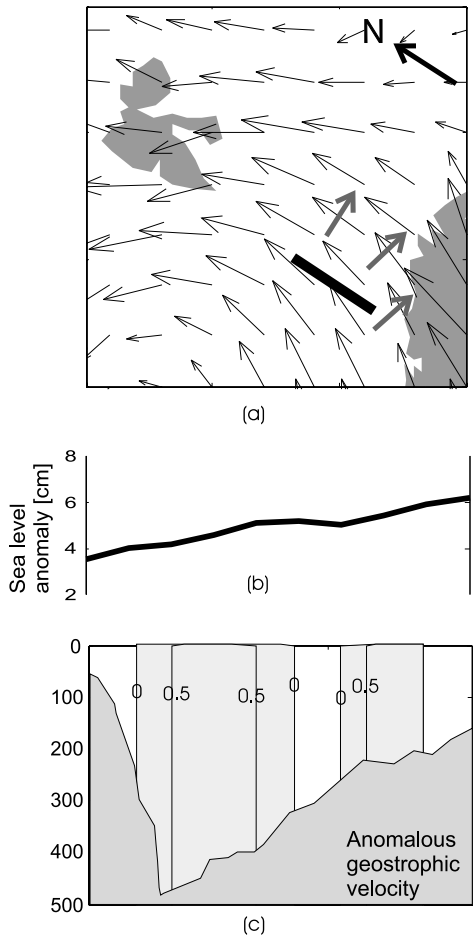

Figure 9. Mean characteristics associated with strong occurrences of the positive EOF1. (a) Horizontal fields of anomalous wind, where the associated Ekman transport also are sketched. Location of mooring array is indicated. (b) Vertical view of modeled sea level anomaly (cm) across the BSO and (c) calculated geostrophic velocities (cm s^{-1}) associated with the sea level in Figure 9b. Shaded areas show eastward flow. For description of the selection criteria, see the text and Figure 8b.

reproduce mainly the pattern of the positive state of EOF1 (Figure 9c), although not completely. The mismatch may be related to an underestimation of the sea level magnitude (see section 2), and the fact that the numerical model includes additional processes.

[15] The wide outflow as described by the negative state of EOF1 (Figure 10a) is characterized by strong northerly winds east of Spitsbergen, northeasterly winds at the section, and southeasterly winds southwest of Spitsbergen. This gives an accumulation of water in the north, consistent with the mean sea level anomaly at times for dominating negative EOF1 (Figure 10b). The geostrophic currents associated with the sea level anomaly resemble the pattern of the negative state of the EOF1 (Figure 10c), although with a mismatch as for the positive EOF1.

[16] In summary, the statistical analysis clearly indicates that the anomalous velocity field across the BSO to a large degree is forced by sea level changes within the section. The sea level changes are created by an accumulation of water induced by the local wind field through the Ekman transport.

4.2. Relations Between the Statistical Analysis and the Observed Flow

[17] The results from section 4.1 showed that when southerly winds prevail (southwesterlies along the Norwegian coast), the anomalous flow is dominated by a wide core of inflow occupying the entire section. Alternatively, when northerly winds prevail, the anomalous flow is dominated by an outflow that occupies the entire section. To relate this to the observed flow, it must be considered as to how the anomalous flow field (Figure 8a) modifies the mean field (Figure 5). When the positive state of EOF1 is dominating, the Atlantic inflow in general is increased, especially within the core at 72°30′N. This is seen clearly in the reconstructed EOF1 at the strongest positive occurrences (Figure 11a). Alternatively, when the negative state of EOF1 is dominating, the outflow in the northern part is increased and the inflow in the southern part is decreased. The largest

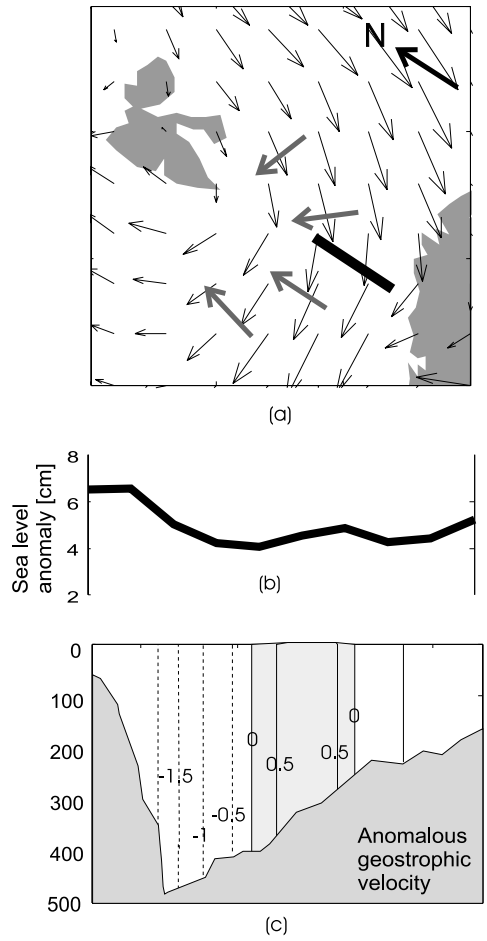

Figure 10. Mean characteristics associated with strong occurrences of the negative EOF1. (a) Horizontal fields of anomalous wind, where the associated Ekman transport also is sketched. Location of mooring array is indicated. (b) Vertical view of modeled sea level anomaly (cm) across the BSO, and (c) calculated geostrophic velocities (cm s^{-1}) associated with the sea level in Figure 10b. Shaded areas show eastward flow. For description of the selection criteria, see the text and Figure 8b.

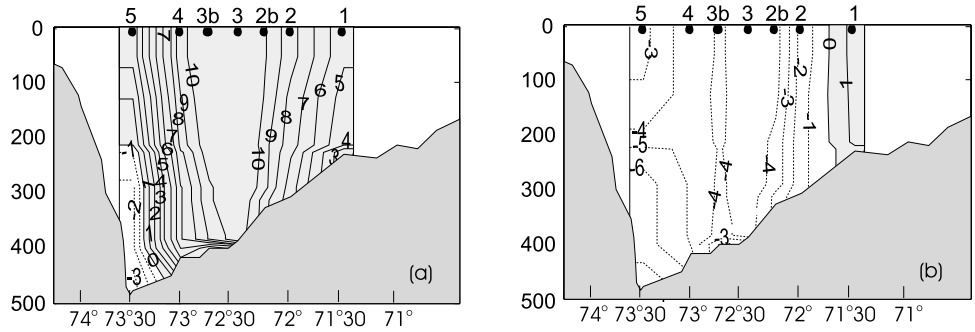

Figure 11. Reconstructed velocity field (cm s^{-1}) from the strong occurrences of EOF1 for the (a) positive state and (b) negative state. Shaded areas show eastward flow. The selection criteria are the same as used in Figures 9 and 10.

decrease is found near 72°30′N. When the flow of the negative EOF1 is strong enough to reverse the current in this area, as it does for the strongest negative occurrences (Figure 11b), it will represent the observed situations of a wide outflow occupying large parts of the section with an inflow only in the southern parts. An example of this may be seen in Figure 4b. A similar situation existed in April 1998 as described by *Ingvaldsen et al.* [2002]. This is consistent with the principal component being negative in most of April 1998 (Figure 8b). Actually, the principal component of EOF1 is also negative in March–April 1999 and 2001, which is consistent with the findings of *Ingvaldsen et al.* [2004], who found a pronounced minimum in the Atlantic inflow (or could even be the outflow) in spring due to an annual event of northerly winds.

4.3. Relations Between the Flow and the Regional Atmospheric Fields

[18] Although a relation between the velocity field and the local wind field is established, the wide inflows and outflows are at times persistent for several weeks. Such a persistency can only be caused by a persistent pattern in the regional wind field. The mean regional atmospheric pressure and wind fields for the positive EOF1 (Figure 12a) show strong similarities with the mean winter situation with the well-known Icelandic low that stretches as a trough into the Nordic Seas. This suggests that persistent wide inflows are a manifestation of the northward extension of the Icelandic low.

[19] The mean regional atmospheric pressure and the wind field for the negative EOF1 (Figure 12b) reveals that the northerly winds that cause the wide outflows are associated with a strong high-pressure area in the Arctic that stretches toward Spitsbergen. This suggests that persistent wide outflows are forced from the Arctic Ocean. The northerly winds move large amounts of water from the Arctic to the northern and eastern Barents Sea, therefore pushing the entire water masses of the northern and eastern Barents Sea southward. The supply of water into the Barents Sea from the Arctic Ocean and a southward movement of the northern and eastern Barents Sea can

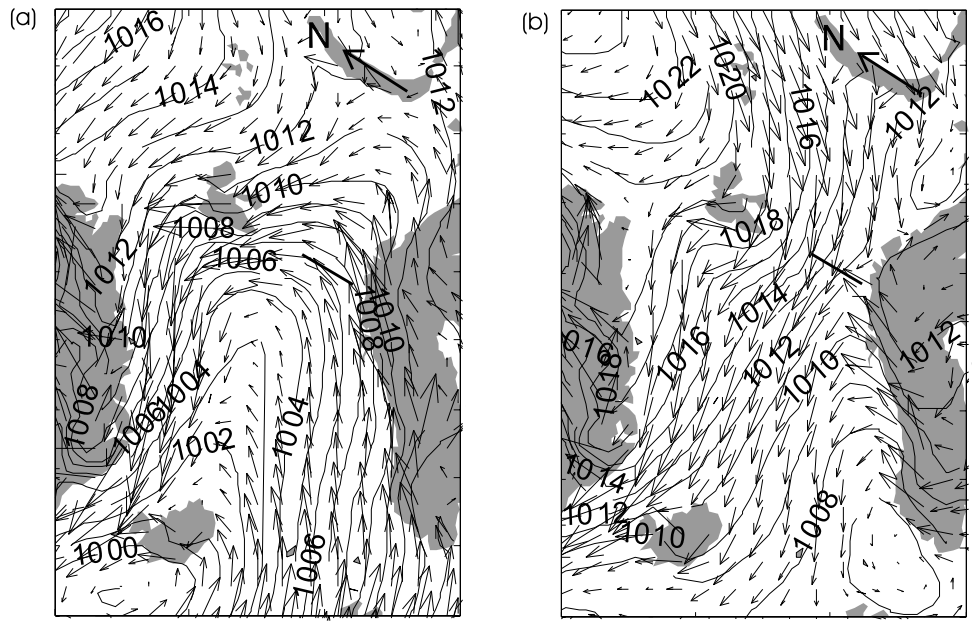

Figure 12. Wind and atmospheric pressure fields associated with the strong occurrences of (a) the positive EOF1 and (b) the negative EOF1. The selection criteria are the same as used in Figures 9 and 10. Location of mooring array is indicated.

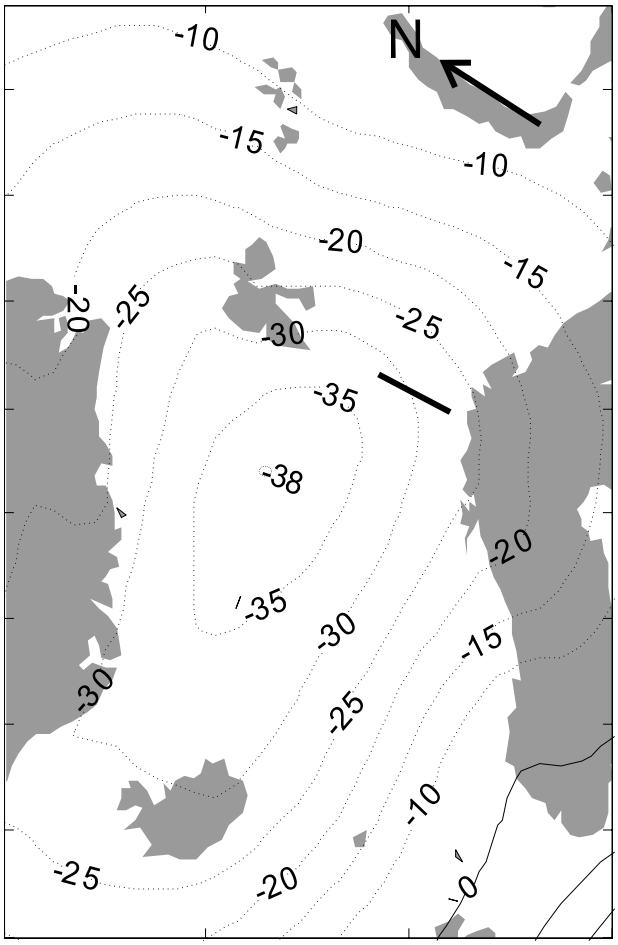

Figure 13. Correlation coefficients (multiplied by 100) between the principal component of EOF1 and atmospheric pressure. Location of mooring array is indicated.

explain why the large outflows can be present for 2–3 weeks without losing too much water through the BSO during this period. It is also consistent with the necessity for a response time between wind and sea level for such a large-scale movement. This could explain why the temperature in the BSO does not decrease significantly during periods of large outflows (e.g., April 1998 in Figure 6), as the outflowing water will come from the southern parts of the Barents Sea and not from the northern parts as it would if it was purely wind driven.

[20] The previous results indicate that the wide inflows and outflows across the BSO are related to the relative strength of the Icelandic low and the Arctic high. However, the correlation coefficient between the principal component of EOF1 and the regional atmospheric pressure field shows that the strongest correlation (−0.38) is found in an area west of the BSO (Figure 13). This probably reflects that this area is a good index for the alignment of the isobars across the BSO, as the local alignment of the isobars decides the local wind field in the BSO. The alignment of the isobars depends on the relative strength of the Icelandic low and the Arctic high, on their lateral extent (i.e., stretching into the Nordic Seas or toward Spitsbergen), and on local processes that are not captured by these large-scale systems. The result should be interpreted as that a strong Icelandic low, stretching into the Nordic Seas, creates the persistent southerly winds necessary for a persistent wide inflow (and vice versa for the outflow), but the details of the velocity field are determined by local effects that are not captured by the regional field.

4.4. Discussion of the Method

[21] The correlation coefficients in Figure 13 are not very high, and higher numbers were desirable to give more quantitative results. To quantify the results, a number of different analyses (including coherence analysis and cross-spectral analysis) between the EOF 1 principal component and a number of different atmospheric parameters (e.g., wind, wind stress, wind shear, atmospheric pressure, etc.) have been performed. Unfortunately, none of them has given instructive results. The reason for this is threefold. First, it is a limitation of the methods used. While conventional EOF analysis works best when variability is over a broad range of frequencies, spectral analysis works best when the variability is in narrow frequency bands. Consequently, the two methods may not necessarily give good results on the same data set. The advantage of EOF analysis is that it provides a compact description of the spatial and temporal variability of data series. However, every method has its limitations, and it is for the spatial analysis of data fields conventional EOF analysis has its greatest advantages. As the motivation for this study primarily was to investigate the spatial distribution of the velocity field, we find this an adequate method, although it may prevent detailed studies of the temporal variability.

[22] Second, the problem may be associated with the performed time filtering of the data material. There are, in general, some disadvantages of applying a 14-day filter before the analysis, as a large portion of the wind effects then will be filtered out. The timescale of an individual passing low-pressure system is 3–7 days, which can make it hard to identify which aspect of the wind forcing is discussed. In addition, the oceanic response to wind field changes occurs on inertial timescales. It could therefore be argued that it is more physically correct to apply the analysis on daily values without any filtering. In that case, the Ekman dynamics may, in fact, explain a larger fraction of the variability, and higher correlation coefficients between the atmospheric fields and the first principal component could maybe be obtained. The problem with this is due to the limited spatial resolution; the current meter data are not reliable enough for a detailed analysis of the spatial structures on less than 14-day timescales. If the detailed analysis were performed without filtering, the Ekman dynamics would still be present but would be obscured by other mesoscale variability that were not properly resolved with the current meter recordings (or in the rather coarse atmospheric fields). The results would be impossible to interpret in detail. However, we still find it instructive to display daily fields to show the patterns in the velocity field and that the Ekman effect is directly visible in the original data (together with other effects). This makes us more confident in the results from the statistical analysis. What the method with time filtering has provided is a possibility of identifying reliable structures in the velocity field, although the spatial resolution is somewhat coarse, and of identifying the spatially distributed atmo-

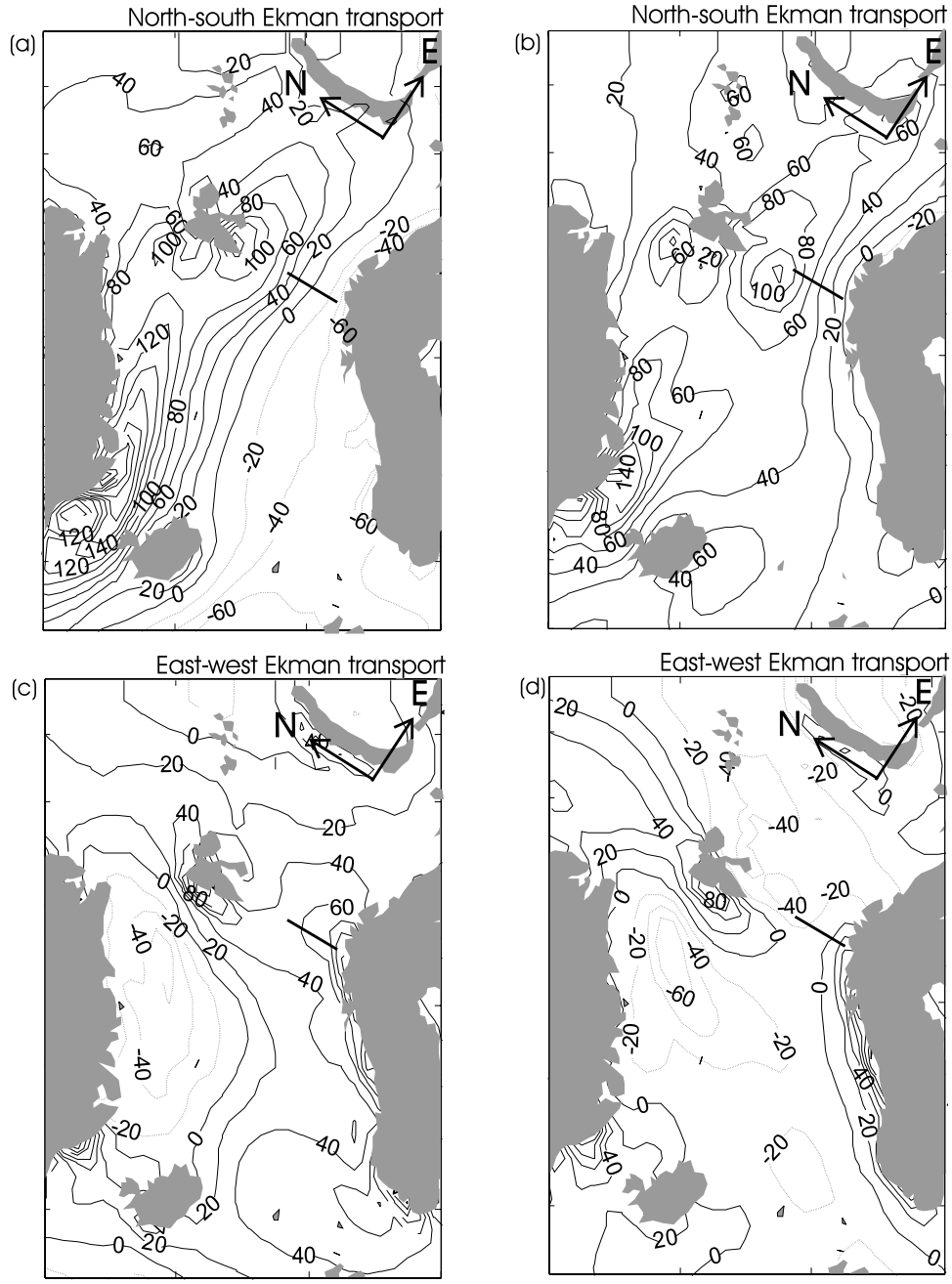

Figure 14. North-south Ekman transport (multiplied by 100 m^2 s^{-1}) associated with the strong occurrences of the (a) positive EOF1 and (b) negative EOF1. East-west Ekman transport associated with the strong occurrences of the (c) positive EOF1 and (d) negative EOF1. The selection criteria are the same as used in Figures 9 and 10. Location of mooring array is indicated.

spheric fields associated with them. Although the ocean responds to wind changes of inertial timescales, it does not mean that this response is filtered out on 14-day timescales.

[23] Third and most importantly, the general problem of quantifying the results is due to the problem of finding a quantitative measure of the relevant atmospheric forcing. It is the spatial distribution of the wind field that causes the effect (i.e., westerly winds in the southern part of the BSO and at the same time easterly winds in the north). Moreover, it is the spatial distribution of the east-west wind component that causes the wide inflows and the spatial distribution in the north-south wind component that causes the wide outflows. This is evident when computing the horizontal Ekman transport associated with the strong occurrences of the positive and negative EOF1. The instantaneous and vertically integrated Ekman transport has north-south components V_E and east-west components U_E given by

$$V_E = -\frac{1}{\rho_0 f}\tau^x$$

$$U_E = \frac{1}{\rho_0 f}\tau^y,$$

where ρ_0 (1026 kg m^{-3}) is the density of seawater and f ($1.39 \cdot 10^{-4}$ s^{-1}) is the Coriolis parameter. The east-west (τ^x) and north-south (τ^y) wind stress were obtained from the east-west ($\vec{u}$) and north-south ($\vec{v}$) wind velocity by

$$\tau^x = \rho_{\text{air}} C_d |\vec{u}| \vec{u}$$

$$\tau^y = \rho_{\text{air}} C_d |\vec{v}| \vec{v},$$

where ρ_{air} (1.3kg m^{-3}) is the density of air and C_d is the drag coefficient as given by *Large and Pond* [1981]. The results are shown in Figure 14. When the wide inflows (the positive EOF1) dominate, the north-south Ekman transport (associated with the east-west wind) is negative in the southern BSO and positive in the northern BSO (Figure 14a) giving the effect described in section 4.1. The east-west Ekman transport (associated with the north-south wind) only shows a gradient close to the Norwegian Coast (Figure 14c). When the wide outflows (the negative EOF1) dominate, the north-south Ekman transport (associated with the east-west wind) is positive across the BSO (Figure 14b). The east-west Ekman transport (associated with the north-south wind), on the other hand, is positive west of the northern BSO and negative east of the northern BSO (Figure 14d) which will accumulate water in the northern BSO as described in section 4.1.

[24] The above results show the difficulty of finding a quantitative measure of the relevant atmospheric forcing. No matter what kind of parameter (wind, wind stress, wind shear, or atmospheric pressure) or key direction is used, the forcing in one single point, or the directional difference between single points, cannot capture the variability needed. As an attempt to capture the spatial distribution of the atmospheric field, EOF analysis on the atmospheric parameters was also applied, but this method did not separate the variability in the spatial structures needed for our explanation model. Unfortunately, this means that it is quite difficult to quantify the conclusions.

5. Summary and Conclusions

[25] By using data from moored current meters between 71°30′N and 73°30′N in a section across the BSO from August 1997 to August 2001, the velocity fields in the AW inflow to the Barents Sea have been examined. In general, the velocity field is dominated by frequent and large fluctuations, and nearly complete reversals of the currents through parts of the section may occur within 1–2 days.

[26] The velocity field was decomposed by EOF analysis and related to the wind field, the sea level height as obtained by numerical modeling, and atmospheric sea level pressure. The key parameter that to a large degree determines the spatial structure of the velocity field is sea level changes that are induced by the local wind field. The main process is the Ekman transport through its ability to accumulate water within the section thereby creating barotropic pressure gradients and associated geostrophic currents. This process is enhanced by the topographic constraints with the Norwegian coast in the southern part.

[27] The mean velocity field shows that the Atlantic inflow takes place as a wide core occupying most of the section between 71°30′N and 73°30′N (except in the deeper parts of the Bear Island Trough). Southwesterly winds along the Norwegian coast and southeasterly winds farther north modulates this velocity field by accumulating surface water in the southern part and at the same time moves the surface waters of the northern areas out of the section. The result is a pressure gradient, which creates a geostrophic velocity field that enhances the wide inflow. When the predominant wind direction is northerly, the Ekman transport will produce a higher water level in the north than in the south. The associated pressure gradient drives a relatively strong outflow in the northern part, often in combination with a weaker inflow in the south. The flow regimes may be persistent for several weeks and are related to the relative strength and lateral extension of the Icelandic low and the Arctic high, but local processes that are not captured by the regional fields determine the details of the flow.

[28] **Acknowledgments.** The results presented have partly been obtained through funding from the European Union MAST III VEINS programme and MAIA project. In addition, funding has come from the Research Council of Norway through the projects "Variation in space and time of cod and other gadoids: The effect of climate and density dependence on population dynamics" and NOClim. Thanks go to Peter Haugan and Øystein Skagseth and two anonymous reviewers for careful reading of the manuscript.

References

Ådlandsvik, B., and R. Hansen (1998), Numerical simulation of the circulation in the Svalbard Bank area in the Barents Sea, *Cont. Shelf Res.*, *18*, 341–355.

Ådlandsvik, B., and H. Loeng (1991), A study of the climatic system in the Barents Sea, *Polar Res.*, *10*(1), 45–49.

Asplin, L., R. Ingvaldsen, and H. Loeng, and B. Ådlandsvik (1998), Description and validation of a 3-dimensional numerical model of the Nordic and Barents Seas, *Fisken og Havet Rep. 10*, 35 pp., Inst. of Mar. Res., Bergen, Norway.

Blindheim, J. (1989), Cascading of Barents Sea bottom water into the Norwegian Sea, *Rapp. P. V. Réun. Cons. Int. Explor. Mer*, *188*, 49–58.

Blumberg, A. F., and G. L. Mellor (1987), A description of a three-dimensional coastal ocean model, in *Three-Dimensional Coastal Ocean Models, Coastal and Estuarine Ser.*, vol. 4, edited by N. Heaps, pp. 1–16, AGU, Washington, D. C.

Eide, L., M. Reigstad, and J. Guddal (1985), Database av beregnede vind og bølgeparametere for Nordsjøen, Norskehavet og Barentshavet hver 6: Time for årene 1955–1981, report, 35 pp., Norw. Meteorol. Inst., Oslo.

Emery, W. J., and R. E. Thomson (1997), *Data Analysis Methods in Physical Oceanography*, Pergamon, New York.

Engedahl, H. B., B. Adlandsvik, and E. Martinsen (1998), Production of monthly mean climatological archives for the Nordic Seas, *J. Mar. Syst.*, *14*, 1–26.

Furevik, T. (1998), On the Atlantic Water flow in the Nordic Seas: Bifurcation and variability, Ph.D. thesis, 218 pp., Univ. of Bergen, Bergen, Norway.

Furevik, T. (2001), Annual and interannual variability of the Atlantic Water temperatures in the Norwegian and Barents Seas: 1980–1996, *Deep Sea Res., Part I*, *48*, 383–404.

Haugan, P. (1999), On the transports of mass, heat and carbon in the Arctic Mediterranean, Ph.D. thesis, 166 pp., Univ. of Bergen, Bergin, Norway.

Ingvaldsen, R., H. Loeng, and L. Asplin (2002), Variability in the Atlantic inflow to the Barents Sea based on a one-year time series from moored current meters, *Cont. Shelf Res.*, *22*, 505–519.

Ingvaldsen, R., H. Loeng, and L. Asplin (2004), The seasonal cycle in the Atlantic inflow to the Barents Sea, *Cont. Shelf. Res.*, in press.

Large, W. G., and S. Pond (1981), Open ocean momentum flux measurements in moderate to strong winds, *J. Phys. Oceanogr.*, *11*, 324–336.

Li, S., and T. A. McClimans (1998), The effects of winds over a barotropic retrograde slope current, *Cont. Shelf Res.*, *18*, 457–485.

Loeng, H., and R. Sætre (2001), Features of the Barents Sea circulation, *Fisken og Havet Rep. 1*, 40 pp., Inst. of Mar. Res., Bergen, Norway.

Loeng, H., V. Ozhigin, and B. Ådlandsvik (1997), Water fluxes through the Barents Sea, ICES, *J. Mar. Sci.*, *54*, 310–317.

McClimans, T. A., B. O. Johannessen, and T. Jenserud (1999), Monitoring a shelf edge current using bottom pressures or coastal sea-level data, *Cont. Shelf Res.*, *19*, 1265–1283.

North, G. R., T. L. Bell, R. F. Cahalan, and F. J. Moeng (1982), Sampling errors in the estimation of empirical orthogonal functions, *Mon. Weather Rev.*, *110*, 699–706.

O'Dwyer, J., Y. Kasajima, and O. A. Nøst (2001), North Atlantic Water in the Barents Sea opening, 1997 to 1999, *Polar Res.*, *20*(2), 209–216.

Roberts, J., and T. D. Roberts (1978), Use of Butterworth low-pass filter for oceanographic data, *J. Geophys. Res.*, *83*, 5510–5514.

Skogen, M., and H. Søiland (1998), A user guide to NORWECOM v2.0, the Norwegian, 1998, Ecological Model System, *Fisken og Havet Rep. 18*, 42 pp., Inst. of Mar. Res., Bergen, Norway.

L. Asplin, R. B. Ingvaldsen, and H. Loeng, Institute of Marine Research, P.O. Box 1870 Nordnes, N-5817 Bergen, Norway. (lars.asplin@imr.no; randi.ingvaldsen@imr.no; harald.loeng@imr.no)